Brain-derived neurotrophic factor knock-out mice develop nonalcoholic steatohepatitis

Running title: BDNF-KO mice develop NASH

Mayuko Ichimura-Shimizu[1] E-mail: ichimura.mayuko@tokushima-u.ac.jp

Masami Kojima[2, 3*] E-mail: masamikojima@neptune.kanazawa-it.ac.jp

Shingo Suzuki [4,5] E-mail: ssuzukineurosci@gmail.com

Misaki Miyata[2] E-mail: b1925115@planet.kanazawa-it.ac.jp

Yui Osaki [1] E-mail: c202001095@tokushima-u.ac.jp

Konomi Matsui [3] E-mail: bdnfpropeptide@gmail.com

Toshiyuki Mizui [3] E-mail: toshi.mizui0820@gmail.com

Koichi Tsuneyama [1] E-mail: tsuneyama.koichi@tokushima-u.ac.jp

[1] Department of Pathology and Laboratory Medicine, Tokushima University Graduate School, 3-18-15 Kuramoto-cho, Tokushima 770-8503, Japan

[2] Department of Applied Bioscience, College of Bioscience and Chemistry, Kanazawa Institute of Technology, 3-1 Yatsukaho, Hakusan, Ishikawa 924-0838, Japan

[3] Biomedical Research Inst., National Institute of Advanced Industrial Science and Technology (AIST), 1-8-31 Midorioka, Ikeda, Osaka, 563-8577, Japan

[4] Department of Anatomy and Neurobiology, Faculty of Medicine, Kagawa University, 1750-1 Ikenobe, Kitagun-Mikicho, Kagawa 761-0701, Japan

[5] Health and Medical Research Inst., National Institute of Advanced Industrial Science and Technology (AIST), 2217-14 Hayashi-cho, Takamatsu, Kagawa 761-0395, Japan

*Correspondence: Masami Kojima

Department of Applied Bioscience, College of Bioscience and Chemistry, Kanazawa Institute of Technology, 3-1 Yatsukaho, Hakusan, Ishikawa 924-0838, Japan

Tel. +81-76-274-8259

E-mail: masamikojima@neptune.kanazawa-it.ac.jp

Disclosure of conflict of interest

The authors declare that they have no conflicts of interest.

Word count: 3994

Abstract

While brain-derived neurotrophic factor (BDNF), which is a growth factor associated with cognitive improvement and the alleviation of depression symptoms, is known to regulate food intake and body weight, the role of BDNF in peripheral disease is not fully understood. Here, we show that reduced BDNF expression is associated with weight gain and the chronic liver disease nonalcoholic steatohepatitis (NASH). At 10 months of age, BDNF-heterozygous ($BDNF^{+/-}$) mice develop symptoms of NASH: centrilobular/perivenular steatosis, lobular inflammation with infiltration of neutrophils, ballooning hepatocytes, and fibrosis of the liver. Obesity and higher serum levels of glucose and insulin—major pathologic features in human NASH—are dramatic. Dying adipocytes are surrounded by macrophages in visceral fat, suggesting that chronic inflammation occurs in peripheral organs. RNA-seq studies of the liver revealed that the most significantly enriched gene ontology term involves fatty acid metabolic processes and the modulation of neutrophil aggregation, pathologies that well characterise NASH. Gene expression analysis by RNA-seq also suggested that the $BDNF^{+/-}$ mice are under oxidative stress, as indicated by alterations in the expression of the cytochrome P450 family and a reduction in glutathione S-transferase p, an antioxidant enzyme. Histopathologic phenotypes of NASH were also observed in a knock-in mouse ($BDNF^{+/pro}$), in which the precursor BDNF is inefficiently converted into the mature form of BDNF. Lastly, as BDNF reduction causes overeating and subsequent obesity, a

food restriction study was conducted in *BDNF*$^{+/pro}$ mice. Pair-fed *BDNF*$^{+/pro}$ mice developed hepatocellular damage and showed infiltration of inflammatory cells including neutrophils in the liver, despite having body weights and blood parameters that were comparable to controls. Collectively, this is the first report demonstrating that reduced BDNF expression plays a role in the pathogenic mechanism of NASH, which is a hepatic manifestation of metabolic syndrome.

Key words: brain-derived neurotrophic factor, nonalcoholic steatohepatitis, nonalcoholic fatty liver disease, liver fibrosis, RNA-seq, gene ontology, mouse model

Introduction

Although fatty liver is typically free of inflammation, 10–20% of patients with fatty liver develop inflammation and fibrosis, which is referred to as nonalcoholic steatohepatitis (NASH) [1]. NASH is a complex and heterogeneous disease involving visceral obesity, type 2 diabetes mellitus, hypertension, hyperglycaemia, and hyperlipidaemia. Furthermore, it has been shown that the intracellular/extracellular events elicited during the progression of NASH occur in the liver and other tissues, including adipose tissue and the intestines [1]. Thus, due to the complex and heterogeneous nature of NASH, a hypothesis known as the 'multiple parallel hits model' has been proposed to explain the pathogenesis of NASH [1]. In the context of drug discovery and treatment of NASH, studies are actively exploring and generating animal models that closely resemble the pathological features observed in humans. Like leptin, brain-derived neurotrophic factor (BDNF), which was originally identified as a growth factor that promotes neuronal survival, differentiation, and synaptic plasticity in the brain [2], governs eating behaviour and energy metabolism through hypothalamic neurons [3]. Mice lacking one allele of the *Bdnf* gene exhibit a tendency toward obesity [3-5]. BDNF binds to the receptor, tropomyosin receptor kinase B (TrkB). In humans, *de novo* missense mutations in the *Trkb* gene result in hyperphagia, severe obesity, and developmental delay [6]. Given this evidence, it is considered that impairment of BDNF function might lead to deficiencies in peripheral organs and/or the

development of peripheral diseases. In this study, we used two distinct mouse lines with decreased BDNF levels and a diet-restriction protocol to investigate the association between reduced BDNF expression and the development of NASH, which represents the hepatic manifestations of metabolic syndrome.

Materials and Methods

Mice

BDNF knock-out mice [7] were kindly provided by Regeneron Pharmaceuticals (Tarrytown, NY, USA) and maintained in a C57BL/6 background, as described previously [8,9]. proBDNF knock-in (*BDNF*$^{+/pro}$) mice were purchased from BioSafety Research Center (Shizuoka, Japan). To generate *BDNF*$^{+/-}$ and *BDNF*$^{+/+}$ littermates, male and female mice with the *BDNF*$^{+/-}$ genotype were intercrossed, and at 6 weeks of age, genotyping was performed as described below. Two male siblings with the genotypes *BDNF*$^{+/-}$ and *BDNF*$^{+/+}$ were housed in the same cage until the indicated age and used for experiments. *BDNF*$^{+/pro}$ and *BDNF*$^{+/+}$ littermates were similarly prepared. The mice had access to a normal diet (MF; Oriental Yeast, Tokyo, Japan) and water ad libitum, except during the pair-feeding experiment. Individually housed *BDNF*$^{+/pro}$ mice were pair-fed to restrict food consumption to the levels of *BDNF*$^{+/+}$ mice from 6 to 16 weeks of age. Mice were maintained at 22–24°C and a relative humidity of 50–60% under a 12-h dark/12-h light cycle. At 10 months old, the mice were fasted overnight (i.e., from 21:00

to 9:00) and sacrificed under anaesthesia. Blood samples were collected from the inferior vena cava. Serum samples obtained were kept at −20°C. Liver and epididymal fat pad were removed, washed in cold saline, and weighed. The liver was frozen immediately in liquid nitrogen and stored at −80°C. Remaining liver tissue portions and adipose tissue were fixed in 10% neutral buffered formalin. All animal experiments were performed in strict accordance with protocols approved by the Animal Use Committee of Tokushima University (Approval No. T30-32) and the Institutional Animal Care and Use Committee of AIST (Approval No. 2019-084), and the animals were maintained in accordance with the guidelines for the care and use of laboratory animals at AIST and Tokushima University. All efforts were made to minimise animal suffering and reduce the number of animals used.

Genotyping

Genotyping of the *BDNF*$^{+/-}$ and *BDNF*$^{+/pro}$ mice was performed by PCR with the following primers. *BDNF*$^{+/-}$ mice: the forward and reverse primers were 5′-ATGAAAGAAGTAAACGTCCAC-3′, 5′-GGGAACTTCCTGACTAGGGG-3′. *BDNF*$^{+/pro}$ mice: the PCR reaction with 5′-TGCACCACCAACTGCTTAG-3′ and 5′-GGATGCAGGGATGATGTTC-3′ generates 550- and 320-bp DNA fragments from wild-type and mutant alleles, respectively [10].

Immunoblotting

For western blotting, hippocampal tissues were homogenised in cold lysis buffer consisting of 50 mM Tris-HCl (pH 7.4), 1 mM EDTA, 150 mM NaCl, 10 mM NaF, 1 mM Na_3VO_4, 1% Triton X-100, 10 mM $Na_2P_2O_7$, 100 µM phenylarsine oxide, and 1% protease inhibitor cocktail (Complete Mini; Roche Diagnostics, Hertfordshire, UK). The lysed tissues were incubated at 4°C for 20 min and then centrifuged at 15,000 rpm for 15 min. Levels of protein in the supernatants were determined using the BCA protein assay kit (Pierce/Thermo Fisher Scientific, Rockford, IL, USA). The lysates (30 µg) were boiled for 5 min at 100°C, electrophoresed on 20% SDS-polyacrylamide gels, and then transferred onto polyvinylidene fluoride membranes (Immobilon P; Millipore, Billerica, MA, USA). The membranes were blocked with TBS containing 0.2% Tween-20 (TBST) and 5% BSA, incubated with a mouse anti–pan-BDNF antibody (clone 3C11; Icosagen, Õssu, Estonia) and a monoclonal β-actin antibody (clone: AC15; Sigma, USA) in TBST containing 0.5% BSA at room temperature for 90 min, and then washed with TBST. Subsequently, the membranes were incubated at room temperature for 30 min with peroxidase-conjugated secondary antibodies in TBST containing 5% BSA and washed with TBST. Signals were detected using ImmunoStar Reagents (Wako, Tokyo, Japan) or SuperSignal WestFemto Maximum Sensitivity Substrate (Thermo Fisher Scientific). The exposure time was adjusted such that the intensity of the bands was within the linear range. The blots were scanned and the images converted to TIFF

files to quantify the intensity of BDNF bands using the NIH ImageJ software (version 1.37v).

Serum biochemical analysis

Serum triglyceride, total cholesterol, glucose, alanine aminotransferase (ALT) and aspartate aminotransferase (AST) levels were determined using a Triglyceride E test Wako, Cholesterol E test Wako, Glucose C II test Wako, and Transaminase C II test Wako (Fujifilm Wako Pure Chemical Industries, Osaka, Japan), respectively. Serum insulin and leptin levels were measured using a Mouse Insulin and Leptin ELISA kit, respectively (Morinaga Institute of Biological Science, Yokohama, Japan).

Histopathological examinations

Paraffin-embedded tissue cut to 2 μm thickness was stained with H&E, and Azan-Mallory. Frozen sections of liver tissue were stained with Oil red O. All histopathologic examinations were performed by a pathologist (K.T.) who was blinded to the experimental and serologic data. Liver histologic findings were scored using the NASH Clinical Research Network Scoring System based on four semi-quantitative factors: steatosis (0–3), lobular inflammation (0–3), hepatocyte ballooning (0–2), and fibrosis (0–4). The nonalcoholic fatty liver disease (NAFLD) activity score was defined as the unweighted sum of the scores for steatosis, lobular inflammation, and hepatocyte

ballooning [11].

Liver and adipose tissues were immunostained for Mac-2 (galectin-3) and myeloperoxidase (MPO) to identify macrophages and neutrophils, respectively. Formalin-fixed tissue slices were deparaffinised, microwaved for 12 min to retrieve antigen, and endogenous peroxidase was blocked with H_2O_2. Non-specific reactions were blocked with TBS containing 5% BSA, followed by incubation of the slices with primary rat monoclonal anti–Mac-2 antibody (1:800, CL8942AP, Cedarlane, Burlington, NC, USA) and anti-MPO (1:4, PA1-38240, Thermo Scientific) at 4°C overnight. The slices were washed with PBS and incubated at room temperature for 60 min with a peroxidase-conjugated immune polymer to detect rat monoclonal antibodies (Histofine PO for rats; Nichirei, Tokyo, Japan). After washing with PBS, colour was developed using 3,3'-diaminobenzidine, and the slices were counterstained with haematoxylin. Mac-2–positive cells were counted in a 200× magnification field the crown like-structures (CLS) area per field [12].

RNA-seq analysis

For the RNA-seq analysis, mRNA was purified from total RNA using a NEBNext Poly (A) mRNA Magnetic Isolation Module (New England Biolabs, Ipswich, MA). Library preparation was carried out using the NEBNext Ultra II RNA Library Prep kit (New England Biolabs) with NEB Next Multiplex Oligos for Illumina (New England Biolabs)

according to the manufacturer's instructions. Sequencing and analysis were outsourced to Genewiz (South Plainfield, NJ). Gene differential analysis and gene ontology (GO) enrichment analysis was performed using the Bioconductor package DESeq2 (V1.6.3) and GOSeq (V3.16), respectively. The criteria used for further analysis of genes showing significant differential expression were defined as a fold change ≥2 and q value < 0.05. The q-value, or false discovery rate, represents an adjusted p-value that takes multiple comparisons into account. TopGO analysis was used to generate directed acyclic graph with the top 5 enriched GO terms as primary nodes.

Statistical analysis

All values were expressed as the mean ± SEM. The significance of differences between groups was evaluated using Student's *t*-test, ANOVA or the chi-square test. All analyses were performed using IBM SPSS statistics software, version 24.0 (IBM Co., Somers, NY). *P* values <0.05 were taken to indicate statistical significance.

Results

Prior to investigating the liver, we explored the physical appearance and weight of the body and organs of the *BDNF*$^{+/-}$ mice used in this study. After birth, male *BDNF*$^{+/-}$ and age-matched control mice were maintained under identical housing and feeding conditions for 10 months. As in previous reports [3-5], *BDNF*$^{+/-}$ mice were markedly

obese (Fig. 1A): at 10 months of age, the mean BW of *BDNF*$^{+/-}$ mice (44.9±1.6 g) was 138±5% higher than that of controls (32.5±1.1 g; Fig. 1B). Given the marked change in BW, we examined the tissues and peripheral organs that could be potentially affected. The findings showed that the wet weight of the epididymal fat pad was 249±13% higher in *BDNF*$^{+/-}$ mice (2.26±0.12 g) compared to the control animals (0.91±0.12 g; Fig. 1C). The liver of *BDNF*$^{+/-}$ mice was grossly enlarged and pale in colour (Fig. 1D). Compared to the controls (1.34±0.04 g), the wet weight of the liver was 189±27% higher in *BDNF*$^{+/-}$ mice (2.53±0.36 g) (Fig. 1E).

Histopathologic symptoms of NASH were identified in the livers of *BDNF*$^{+/-}$ mice. In humans, the symptoms of steatohepatitis include the following: hepatocellular steatosis extending from the centrilobular/perivenular region to the periphery; inflammatory cell infiltration, including neutrophils in the hepatic parenchyma; and, ballooning degeneration of damaged hepatocytes [13]. *BDNF*$^{+/-}$ mice exhibited moderate to severe (grade 2 or 3) micro-macrovesicular steatosis with a predominantly centrilobular/perivenular distribution (Fig. 2A). Oil red O staining revealed lipid deposition in hepatocytes. Mild to moderate (grade 2 or 3) focal necrosis was also frequently observed, along with a few ballooning hepatocytes (grade 1 or 2). Immunostaining for MPO, which is associated with neutrophil infiltration and is one of the histopathological features of NASH [14], revealed a pronounced presence in the livers of BDNF$^{+/-}$ mice (Fig. 2B). Conversely, similar significant histopathologic

symptoms were not observed in control animals. All of the *BDNF*$^{+/-}$ mice tested exhibited higher grades and stages of steatosis, lobular inflammation, hepatocyte ballooning and fibrosis in histological assessment (Fig. 2C). The NAFLD activity scores, defined as the unweighted sum of the scores for steatosis, lobular inflammation, and hepatocyte ballooning [11], were ≥5 in all of the *BDNF*$^{+/-}$ mice tested, indicating steatohepatitis in the liver of *BDNF*$^{+/-}$ mice. Interestingly, striking yet mild fibrosis was observed in the livers of *BDNF*$^{+/-}$ mice, and the pathologic lesions resembled those of human NASH, i.e., delicate fibres similar in appearance of chicken wire, typically arising perivenularly and perisinusoidally in the centrilobular/perivenular region (Fig. 2D, E) [15]. The onset of fibrosis is suggestive of persistent inflammation in the liver of *BDNF*$^{+/-}$ mice. Importantly, the histopathological characteristics of the livers of *BDNF*$^{+/-}$ mice had the hallmark features of NASH in humans.

Serum glucose levels in *BDNF*$^{+/-}$ mice were markedly higher than those in control mice (Fig 3A). Serum insulin levels and the insulin-resistance index, calculated using the homeostasis assessment model, were significantly higher in *BDNF*$^{+/-}$ mice (Fig 3B, C). Serum ALT and AST levels were also elevated in *BDNF*$^{+/-}$ mice (Fig 3D, E). However, no significant signs of hyperlipidaemia were observed in *BDNF*$^{+/-}$ mice (Fig 3F, G).

Increases in the size and number of adipocytes are part of the pathological phenotype of obesity [16]. *BDNF*$^{+/-}$ mice exhibited enlarged adipocytes and signs of inflammation, such as the presence of CLS, dead adipocytes surrounded by macrophages stained with

the marker Mac-2 [17] with a CLS density of 527±149% (Fig. 3H, I). Enlarged adipocytes and activated macrophages secrete a variety of cytokines that induce metabolic dysfunction and inflammation [18]. Adipose tissue–derived cytokines are crucial mediators of inflammation in the liver [1,18]. Therefore, we measured the serum levels of the adipocytokines TNF-α and leptin. Although TNF-α levels were under detection limits (data not shown), serum leptin levels were 832±96% higher in *BDNF*$^{+/-}$ mice (31.15±3.60 ng/ml) than in control animals (3.74±0.80 ng/ml; Fig. 3J). Leptin acts directly on the hypothalamus to regulate food intake and energy expenditure, while in peripheral tissues, it functions as an inflammatory adipocytokine [19]. It is therefore suggested that visceral fat inflammation and the inflammatory effects of leptin, which are considered to be important mechanisms for NASH development in humans [20], play a critical role in the development of NASH-like liver pathology in BDNF$^{+/-}$ mice. To explore the molecular mechanisms underlying the development of NASH in *BDNF*$^{+/-}$ mice, we performed a gene ontology study using RNA-seq (database link). A heat map of differentially expressed genes (DEGs) based on fold change shows that there are significant differences in gene expression levels in the livers of *BDNF*$^{+/-}$ and control mice (Fig. 4A). By filtering genes with a fold change ≥2 and q values < 0.05, the total number of DEGs that increased and decreased was 284 and 261, respectively (Fig. 4B). A directed acyclic graph, which is a graphical representation of the results of enrichment analysis of the DEGs, shows the top five enriched GO terms, which included lipid

metabolism processes (GO: 0006629), cellular lipid metabolism (GO: 0044255), and fatty acid metabolism (GO: 0006631) in the “biological processes” GO category (Fig. 4C). Figures 4D and E show the DEGs and GO terms related to relevant biological processes, cellular components, and molecular functions (Fig. 4D), and the top 30 GO terms with *p* values estimated by the enrichment analysis (Fig. 4E), respectively. Since three of the most significantly enriched GO terms were iron ion binding, haem binding, and response to drugs, we first investigated the expression levels of the cytochrome P450 (CYP) family of genes, which are the source of reactive oxygen species (ROS) involved in developing NASH. As shown in Supplementary Table 1, *Cyp2b9* and *Cyp2b13*, which constitute the majority of the *Cyp2b* genes in the liver [21], had markedly increased gene expression levels in $BDNF^{+/-}$ mice compared to the expression levels in the control mice (*Cyp2b9*, p=0.005; *Cyp2b13*, p=0.044). Another source of ROS is neutrophils, which utilise MPO to produce superoxide. The infiltration of MPO-positive neutrophils was observed immunohistochemically in the liver of $BDNF^{+/-}$ mice (Fig. 2B). Conversely, the expression of glutathione S-transferase p1 and 2 (*Gstp1, Gstp2*), which are annotated as “negative regulation of neutrophil aggregation and peroxidase activity and positive regulation of superoxide anion generation” and have the potency to protect cells from oxidative stress, decreased significantly in the livers of the mutant mice (Figure 4F, *Gstp1*: control, 846.6±54.8; $BDNF^{+/-}$, 190.4±11.8; p<0.001; *Gstp2*: control, 5.9±1.1; $BDNF^{+/-}$, 1.1±0.2; p=0.004). Thus, these gene

expression data elucidated by RNA-seq analysis support the indication that BDNF$^{+/-}$ mice developed NASH under oxidative stress, which is a similar pathogenesis to that found in humans.

To further clarify the implication of a reduction in BDNF expression in the development of NASH, a histological study was performed using livers from a genetically engineered mouse line in which the precursor of BDNF is inefficiently converted into the mature form of BDNF [10]. Consistent with our previous report [10], immunoblotting analysis showed that *BDNF*$^{+/pro}$ mice produced approximately half the normal amount of mature BDNF (Fig. 5A). The 10-month-old *BDNF*$^{+/pro}$ mice reared in this study were visibly obese (Fig. 5B), and the weight of body, liver and epididymal fat pad were all higher in the *BDNF*$^{+/pro}$ group than in their *BDNF*$^{+/+}$ littermates (Fig. 5C–E). In addition, the histopathologic phenotypes of NASH were clearly observed in the livers of *BDNF*$^{+/pro}$ mice (Fig. 5F, G). These data suggest that *BDNF*$^{+/pro}$ mice exhibit NASH symptoms most consistently with *BDNF*$^{+/-}$ mice, and that a reduction in BDNF expression could be the pathogenic mechanism underlying NASH development.

Lastly, to exclude the influence of overeating due to a reduction in BDNF, a food restriction study was conducted using *BDNF*$^{+/pro}$ mice. At the beginning of the pair-feeding at 6 weeks of age, there was no significant difference in BW between *BDNF*$^{+/pro}$ mice and controls (data not shown). When *BDNF*$^{+/pro}$ mice were food-restricted for 10 weeks, weight gain was suppressed (Fig. 6A,B). However, ad libitum-fed *BDNF*$^{+/pro}$

mice significantly increased BW (Fig.6C). In the pair-fed *BDNF*$^{+/pro}$ mice, the wet weight of the liver and epididymal fat pad were lower than those in ad libitum-fed *BDNF*$^{+/pro}$ mice (Fig. 6D, E). Serum levels of glucose, insulin, ALT, and triglyceride were lower in pair-fed *BDNF*$^{+/pro}$ mice than in ad libitum-fed *BDNF*$^{+/pro}$ mice, although no significant differences were observed in total cholesterol levels among groups (Fig. 6F–J). Liver histological assessments in *BDNF*$^{+/pro}$ mice showed that 10 weeks of ad libitum feeding resulted in mild steatosis with inflammatory foci, both of which are typical of early NASH. In the pair-fed mice, slightly mild steatosis was accompanied by low BW. However, hepatocellular damage and infiltration of inflammatory cells, including neutrophils, which are characteristic of NASH pathology, were observed in pair-fed *BDNF*$^{+/pro}$ mice (Fig. 6K). Thus, mice with low levels of BDNF that develop NASH in later life had hepatocellular damage, even though their BW and serum metabolic markers were maintained at normal levels by suppressing overeating.

Discussion

Although an increasing number of reports have shown that BDNF dysfunction is associated with the development of various brain disorders, the role of BDNF in peripheral diseases from adulthood to advanced age has been poorly investigated. It has been reported that the activation of BDNF signalling in the hypothalamus controls BW and energy [22]. Mice lacking one allele of the *Bdnf* gene (*BDNF*$^{+/-}$ mice) exhibit a

tendency to develop obesity with hyperphagia [3-5]. The findings of the present study showed that 10-month-old *BDNF*$^{+/-}$ mice fed standard chow exhibit the full spectrum of NASH. These symptoms were identified using robust histological methods, and the molecular and cellular processes underlying the pathology were confirmed using a combination of RNA-seq and gene ontology techniques. As a hepatic manifestation of metabolic syndrome, NASH represents a complex heterogeneous disease. To explain the development of NASH, a hypothesis referred to as the multi-parallel hits model has been proposed, and the pathogenic mechanism of NASH has been explored in extrahepatic tissues as well as in the liver [1,23]. It is considered that that the role of BDNF in the life stages from adulthood to old age is still less understood than its effect during the developmental period of the brain. The findings of the present study suggest that BDNF plays an important role throughout an individual's lifespan and that BDNF dysfunction is a risk factor not only for brain disorders, but also for lifestyle-related peripheral diseases.

BDNF heterozygous mice also exhibited clear signs of hepatic fibrosis, a crucial phenotype that determines prognosis in human NASH. Notably, despite the generation of NASH model animals for several years, the comprehensive phenotypes of NASH including hepatic steatosis, inflammation, and fibrosis, are rarely fully replicated [24,25]. Leptin, like BDNF, suppresses food intake and increases energy expenditure by the body [22]. Leptin knock-out mice exhibit hyperphagic obesity, hepatic steatosis and

inflammation, but not fibrosis [24]. This is because leptin is an essential mediator of fibrogenic effects on the liver [26,27]. Hypothalamic BDNF downregulates leptin synthesis in white adipose tissue via sympathoneural β-adrenergic signalling [28]. Progression to hepatic fibrosis in *BDNF*$^{+/-}$ mice therefore could be explained by increased leptin production in adipocytes secondary to decreased BDNF and its hematogenous effect on the liver. Further, excessive leptin secretion did not suppress appetite and induced obesity in *BDNF*$^{+/-}$ mice. The mechanism underlying this phenomenon is the dependence of the normal action of leptin in the hypothalamus on *Bdnf* transcripts within neurons [29]. The pathogenesis of fibrosis may also involve inflammation of extrahepatic tissues, exemplified by CLS in adipose tissue. Given that macrophages infiltrate and become activated in chronically inflamed tissues [17], hepatic fibrogenesis in the liver of *BDNF*$^{+/-}$ mice might be promoted by pro-inflammatory cytokines [30]. The presence of liver fibrosis in the reduced-BDNF mice suggests that they may differ from a simple overeating-induced NASH model. This finding supports the multiple parallel hits hypothesis of NASH and suggests the involvement of multiple factors in the development of the disease.

Hyperphagia induces obesity and dysfunction in glucose and lipid metabolism, which are risk factors for the development of NASH [24,31]. Previous reports demonstrated that *BDNF*$^{+/-}$ mice exhibit hyperphagia and show increased levels of serum glucose, insulin, and leptin [4,5]. Coppola et al. reported that restricted food intake results in

decreases in BW and serum glucose levels in *BDNF*$^{+/-}$ mice [32]. As reported in a previous study, we found that *BDNF*$^{+/pro}$ mice, which exhibit overeating [10], showed normal levels of BW and serum glucose when food intake was restricted. The livers of these mice presented with suppressed steatosis, but centrilobular hepatocyte damage and neutrophil infiltration were observed, as would be expected in the very early stages of NASH. Despite the chronic nature of hepatitis, the presence of neutrophils in the liver is a significant feature of NASH [14]. It has been reported that the activation of neutrophils mediates the transition from steatosis to steatohepatitis [33]. Considering the existence of lean NASH patients [34], it has become apparent that there is a subtype of NASH that is not dependent on metabolic disorders resulting from hyperphagia or obesity. In this context, BDNF might be a potential contributor to this subtype. Nonetheless, hyperphagia is both a central cause and accelerator of the development of NASH in *BDNF*$^{+/-}$ and *BDNF*$^{+/pro}$ mice.

An interesting question is whether BDNF exerts any direct effects on the liver beyond its role in metabolic regulation through the control of appetite in the hypothalamus. BDNF and its receptor, TrkB, are predominantly synthesised in the brain, but they are also expressed in peripheral metabolic organs such as liver, muscle, pancreas, and adipose tissue [35]. In hepatocytes, BDNF activates signalling pathways such as the enhancement of fatty acid oxidation and the reduction of lipogenesis and gluconeogenesis [35,36]. Nakagawa et al. demonstrated that intracerebroventricular

administration of BDNF to pair-fed obese db/db mice decreased blood glucose levels, suggesting that BDNF can improve glucose metabolism in a manner that is independent of its anorexigenic effect [37]. Passino et al. reported that signalling of p75, known as a low-affinity nerve growth factor receptor, regulates the differentiation of hepatic stellate cells to produce collagen [38]. In addition, it has been reported that the α7 nicotinic acetylcholine receptor (α7nAChR), which is expressed on the surface of macrophages and is partly controlled by BDNF, mediates the inhibition of pro-inflammatory cytokine production and that α7nAChR deficiency exacerbates hepatic inflammation and fibrosis in NASH [39-41]. Further studies on the action of BDNF in different cells in the liver, such as stellate cells and macrophages, could better clarify the pathogenesis of non-hypothalamic-mediated liver injury.

To date, there has been increasing evidence indicating that the *in vivo* role of BDNF is to promote neuronal survival and differentiation during brain development. BDNF has also been implicated in synaptic functioning associated with learning and memory in the adult brain [2]. Moreover, BDNF has been proposed to act as a connection between the central nervous system and peripheral organs through regulating energy intake and expenditure, and to exert pleiotropic effects in the periphery beyond the central nervous system [36,42]. In a cross-sectional study, Hattori et al. recently reported high levels of serum BDNF in NAFLD [43]. The authors of that study speculate that the elevation of serum BDNF levels might be a compensatory response aimed at counteracting abnormal

glucose and lipid metabolism. In addition, Xiong et al. reported that overexpression of BDNF suppresses the onset of NASH [44]. One remaining research challenge is to comprehensively elucidate the specific role of BDNF in the liver and its significance in the pathogenesis of the disease. Our study, which is the first to demonstrate the association between decreased BDNF protein expression and NASH features characterised by metabolic dysfunction and inflammation, offers novel insights into the pathogenesis of NASH. Furthermore, our findings suggest the potential involvement of BDNF in liver-related mechanisms related to NASH.

Author Contributions

M.S., M.K., and K.T. designed the research; M.S., M.K., S.S., M.M., Y.O., K.M., T. M., and K.T. performed the research; M.S., M.T., S.S., M.M., Y.O., K.M., and K.T. performed data validation and analysis; and M.S., M.K., S.S., M.M., T. M., and K.T. prepared the original draft of the manuscript.

Data availability

All data are included in the article and supplementary files, or available from the authors upon reasonable request. Nucleotide sequence data reported are available in the DDBJ Sequenced Read Archive under the accession number E-GEAD-466.

References

1. Tilg H, Moschen AR. Evolution of inflammation in nonalcoholic fatty liver disease: The multiple parallel hits hypothesis. *Hepatology* 2010; **52**: 1836-1846.

2. Bibel M, Barde YA. Neurotrophins: key regulators of cell fate and cell shape in the vertebrate nervous system. *Genes Dev* 2000; **14**: 2919-2937.

3. Kernie SG. BDNF regulates eating behavior and locomotor activity in mice. *The EMBO Journal* 2000; **19**: 1290-1300.

4. Lyons WE, Mamounas LA, Ricaurte GA*, et al.* Brain-derived neurotrophic factor-deficient mice develop aggressiveness and hyperphagia in conjunction with brain serotonergic abnormalities. *Proceedings of the National Academy of Sciences* 1999; **96**: 15239-15244.

5. Rios M, Fan G, Fekete C*, et al.* Conditional deletion of brain-derived neurotrophic factor in the postnatal brain leads to obesity and hyperactivity. 2001; **15**: 1748-1757.

6. Yeo GS, Connie Hung CC, Rochford J*, et al.* A de novo mutation affecting human TrkB associated with severe obesity and developmental delay. *Nat Neurosci* 2004; **7**: 1187-1189.

7. Conover JC, Erickson JT, Katz DM*, et al.* Neuronal deficits, not involving motor neurons, in mice lacking BDNF and/or NT4. *Nature* 1995; **375**: 235-238.

8. Itami C, Kimura F, Nakamura S. Brain-derived neurotrophic factor regulates the maturation of layer 4 fast-spiking cells after the second postnatal week in the

developing barrel cortex. 2007; **27**: 2241-2252.

9. Mizui T, Ishikawa Y, Kumanogoh H*, et al.* BDNF pro-peptide actions facilitate hippocampal LTD and are altered by the common BDNF polymorphism Val66Met. *Proc Nati Acad Sci* 2015; **112**: E3067-E3074.

10. Kojima M, Otabi H, Kumanogoh H*, et al.* Reduction in BDNF from inefficient precursor conversion influences nest building and promotes depressive-like behavior in mice. *Int J Mol Sci* 2020; **21**.

11. Kleiner DE, Brunt EM, Van Natta M*, et al.* Design and validation of a histological scoring system for nonalcoholic fatty liver disease. *Hepatology* 2005; **41**: 1313-1321.

12. Fujimoto M, Tsuneyama K, Fujimoto T*, et al.* Spirulina improves non-alcoholic steatohepatitis, visceral fat macrophage aggregation, and serum leptin in a mouse model of metabolic syndrome. *Dig Liver Dis* 2012; **44**: 767-774.

13. Ludwig J, Viggiano TR, McGill DB*, et al.* Nonalcoholic steatohepatitis: Mayo Clinic experiences with a hitherto unnamed disease. *Mayo Clin Proc* 1980; **55**: 434-438.

14. Wu L, Gao X, Guo Q*, et al.* The role of neutrophils in innate immunity-driven nonalcoholic steatohepatitis: lessons learned and future promise. *Hepatol Int* 2020; **14**: 652-666.

15. Takahashi Y. Histopathology of nonalcoholic fatty liver disease/nonalcoholic steatohepatitis. *World J Gastroenterol* 2014; **20**: 15539.

16. Strissel KJ, Stancheva Z, Miyoshi H*, et al.* Adipocyte Death, Adipose Tissue

Remodeling, and Obesity Complications. 2007; **56**: 2910-2918.

17. Murano I, Barbatelli G, Parisani V*, et al.* Dead adipocytes, detected as crown-like structures, are prevalent in visceral fat depots of genetically obese mice. *J Lipid Res* 2008; **49**: 1562-1568.

18. Duval C, Thissen U, Keshtkar S*, et al.* Adipose Tissue Dysfunction Signals Progression of Hepatic Steatosis Towards Nonalcoholic Steatohepatitis in C57Bl/6 Mice. *Diabetes* 2010; **59**: 3181-3191.

19. Imajo K, Fujita K, Yoneda M*, et al.* Hyperresponsivity to low-dose endotoxin during progression to nonalcoholic steatohepatitis is regulated by leptin-mediated signaling. *Cell Metab* 2012; **16**: 44-54.

20. Du Plessis J, Van Pelt J, Korf H*, et al.* Association of adipose tissue inflammation with histologic severity of nonalcoholic fatty liver disease. *Gastroenterology* 2015; **149**: 635-648.e614.

21. Heintz MM, Kumar R, Rutledge MM*, et al.* Cyp2b-null male mice are susceptible to diet-induced obesity and perturbations in lipid homeostasis. *J Nutr Biochem* 2019; **70**: 125-137.

22. Xu B, Xie X. Neurotrophic factor control of satiety and body weight. *Nat Rev Neurosci* 2016; **17**: 282-292.

23. Tilg H, Adolph TE, Moschen AR. Multiple parallel hits hypothesis in nonalcoholic fatty liver disease: Revisited after a decade. *Hepatology* 2021; **73**: 833-842.

24. Larter CZ, Yeh MM. Animal models of NASH: Getting both pathology and metabolic context right. *J Gastroenterol Hepatol* 2008; **23**: 1635-1648.

25. Sanches SC, Ramalho LN, Augusto MJ*, et al.* Nonalcoholic steatohepatitis: A search for factual animal models. *Biomed Res Int* 2015; **2015**: 574832.

26. Ikejima K, Takei Y, Honda H*, et al.* Leptin receptor–mediated signaling regulates hepatic fibrogenesis and remodeling of extracellular matrix in the rat. *Gastroenterology* 2002; **122**: 1399-1410.

27. Leclercq IA, Farrell GC, Schriemer R*, et al.* Leptin is essential for the hepatic fibrogenic response to chronic liver injury. *J Hepatol* 2002; **37**: 206-213.

28. Cao L, Liu X, Lin E-JD*, et al.* Environmental and Genetic Activation of a Brain-Adipocyte BDNF/Leptin Axis Causes Cancer Remission and Inhibition. *Cell* 2010; **142**: 52-64.

29. Liao G-Y, An JJ, Gharami K*, et al.* Dendritically targeted Bdnf mRNA is essential for energy balance and response to leptin. *Nat Med* 2012; **18**: 564-571.

30. Stanton MC, Chen S-C, Jackson JV*, et al.* Inflammatory signals shift from adipose to liver during high fat feeding and influence the development of steatohepatitis in mice. *J Inflamm* 2011; **8**: 8.

31. Larter CZ, Chitturi S, Heydet D*, et al.* A fresh look at NASH pathogenesis. Part 1: The metabolic movers. *J Gastroenterol Hepatol* 2010; **25**: 672-690.

32. Coppola V, Tessarollo L. Control of hyperphagia prevents obesity in BDNF

heterozygous mice. *Neuroreport* 2004; **15**: 2665-2668.

33. Zang S, Wang L, Ma X*, et al.* Neutrophils play a crucial role in the early stage of nonalcoholic steatohepatitis via neutrophil elastase in mice. *Cell Biochem Biophys* 2015; **73**: 479-487.

34. Younes R, Bugianesi E. NASH in lean individuals. *Semin Liver Dis* 2019; **39**: 086-095.

35. Di Rosa MC, Zimbone S, Saab MW*, et al.* The pleiotropic potential of BDNF beyond neurons: Implication for a healthy mind in a healthy body. *Life* 2021; **11**: 1256.

36. Genzer Y, Chapnik N, Froy O. Effect of brain-derived neurotrophic factor (BDNF) on hepatocyte metabolism. *Int J Biochem Cell Biol* 2017; **88**: 69-74.

37. Nakagawa T, Tsuchida A, Itakura Y, *et al*. Brain-derived neurotrophic factor regulates glucose metabolism by modulating energy balance in diabetic mice. *Diabetes* 2000; **49**: 436-444.

38. Passino MA, Ryan AA, Sikorski SL*, et al.* Regulation of hepatic stellate cell differentiation by the neurotrophin receptor p75NTR. *Science* 2007; **315**: 1853-1856.

39. Massey KA, Zago WM, Berg DK. BDNF up-regulates α7 nicotinic acetylcholine receptor levels on subpopulations of hippocampal interneurons. *Mol Cell Neurosci* 2006; **33**: 381-388.

40. Wang H, Yu M, Ochani M*, et al.* Nicotinic acetylcholine receptor α7 subunit is an essential regulator of inflammation. *Nature* 2003; **421**: 384-388.

41. Kimura K, Inaba Y, Watanabe H*, et al.* Nicotinic alpha‐7 acetylcholine receptor

deficiency exacerbates hepatic inflammation and fibrosis in a mouse model of non‐alcoholic steatohepatitis. *J Diabetes Investig* 2019; **10**: 659-666.

42. Podyma B, Parekh K, Guler AD*, et al.* Metabolic homeostasis via BDNF and its receptors. *Trends Endocrinol Metab* 2021; **32**: 488-499.

43. Hattori Y, Yamada H, Munetsuna E*, et al.* Increased brain-derived neurotrophic factor in the serum of persons with nonalcoholic fatty liver disease. *Endocr J* 2022; **69**: 999-1006.

44. Xiong J, Liu T, Mi L*, et al.* hnRNPU/TrkB Defines a Chromatin Accessibility Checkpoint for Liver Injury and Nonalcoholic Steatohepatitis Pathogenesis. *Hepatology* 2020; **71**: 1228-1246.

Figures legends

Figure 1. Physical appearance, body weight, and weight of epididymal fat pad and liver of 10-month-old male BDNF$^{+/-}$ mice. A. Physical appearance. B-C. Weight of the whole body and epididymal fat pad. D. Gross appearance of liver. E. Liver weight. Number of animals used; 5 (control), 4 (BDNF$^{+/-}$) (B, C, E). Scale bars; 2 cm (A) and 1 cm (D). Values are presented as mean ± SEM. Statistical analysis was performed using the Student's *t*-test.

Figure 2. Liver pathology of 10-month-old BDNF$^{+/-}$ mice. A. Representative H&E and Oil red O staining. Infiltration of inflammatory cells and ballooning hepatocytes, indicated by arrow and arrowheads, respectively. CV, central vein; P, portal tract. B. Myeloperoxidase immunostaining of the liver. C. Histological grade of steatosis, lobular inflammation, ballooning hepatocytes and NAFLD activity score, which was determined as the unweighted sum of the grade for them. D. Representative Azan-Mallory staining. E. Fibrosis stage. Number of animals used; 5 (control), 4 (BDNF$^{+/-}$) (B, D). Statistical analysis was carried out using the chi-square test, with significance shown on each graph. Control (white circles), BDNF$^{+/-}$ (black squares).

Figure 3. Systemic pathology of 10-month-old BDNF$^{+/-}$ mice. A-G. Serum parameters of 10-month-old control and BDNF$^{+/-}$ mice. The insulin resistance index was calculated using the homeostasis model of assessment (serum glucose [mg/dL] × serum insulin [ng/mL]/405). Blood samples were obtained after overnight fasting from 21:00 to 9:00. H. Representative hematoxylin and eosin staining and Mac-2 immunostaining (inset) of epididymal fat pad. I. CLS density in adipose tissue. CLS density was calculated as Mac-2–positive staining area per field at 200× magnification. J. Serum leptin level. Values are presented as mean ± SEM. Number of animals used; 5 (control), 4 (BDNF$^{+/-}$). Statistical analysis was performed using the Student's *t*-test.

Figure 4. Transcriptomic impact of BDNF gene hetero knockout in the liver. A. Heat map of the top 300 genes with high p value. B. A volcano plot representation of significantly up- and down-regulated genes in BDNF$^{+/-}$ mice compared to controls. C. Directed Acyclic Graph with the top 5 GO terms as primary nodes by TopGO analysis. The branch represents the inclusion relation, and the functional range defined from the top to the bottom is in decreasing order. Boxes indicate the 5 most significant terms. Box color represents the relative significance, ranging from dark red (most significant) to light yellow (least significant). Black arrows indicate is a relationships. D. Histogram of the number differentially expressed genes in each GO term with the specification of the relevant biological process, cellular component and molecular function. Shown is

the top 30 most prominent GO categories. E. Histogram of p value of GO enrichment for the top 30 most prominent GO categories. F. RNA expression of *Gstp1* and *Gstp2*. Gene expression and differential expression analysis was carried out using Hisat2, HTseq and DESeq2. Quantitative analysis of expression levels was performed by comparing fragments per kilobase of exon per million reads mapped (FPKM) values.

Figure 5. Systemic and liver pathology of 10-month-old BDNF$^{+/pro}$ mice.

A. Reduced BDNF levels. Hippocampal lysates were prepared from mice of the indicated genotype, and Western blot analysis was performed. Note that BDNF levels were lower in BDNF$^{+/pro}$ animals than controls. B. Physical appearance. C-E. Whole-body weight and weight of the epididymal fat pad and liver. Number of animals used: 5 (BDNF$^{+/+}$), 5 (BDNF$^{+/pro}$) Data are presented as mean ± SEM. F. Representative H&E staining. Infiltration of inflammatory cells and ballooning hepatocytes, indicated by arrow and arrowheads, respectively. CV, central vein; P, portal tract. Note that as with BDNF$^{+/pro}$ mice, BDNF$^{+/pro}$ mice exhibited NASH-like pathology of the liver. G. Representative Azan-Mallory staining.

Figure 6. Systemic and liver pathology of pair-fed BDNF$^{+/pro}$ mice from 6 to 16 weeks of age.

A. Average daily food intake from 6 to 16 weeks of age. B. BW gain calculated as the difference between final and initial BW. C-E. Whole BW and weight of the liver and epididymal fat pad. F-J. Serum parameters. Number of animals used: 5 ($BDNF^{+/+}$), 5 (ad libitum-fed $BDNF^{+/pro}$), 5 (pair-fed $BDNF^{+/pro}$). Values are presented as mean ± SEM. Statistical analysis was performed using ANOVA and Bonferroni's *post hoc* test. K. Representative H&E staining and immunostaining of myeloperoxidase. Infiltration of inflammatory cells indicated by arrows. CV, central vein; P, portal tract.

Figure1

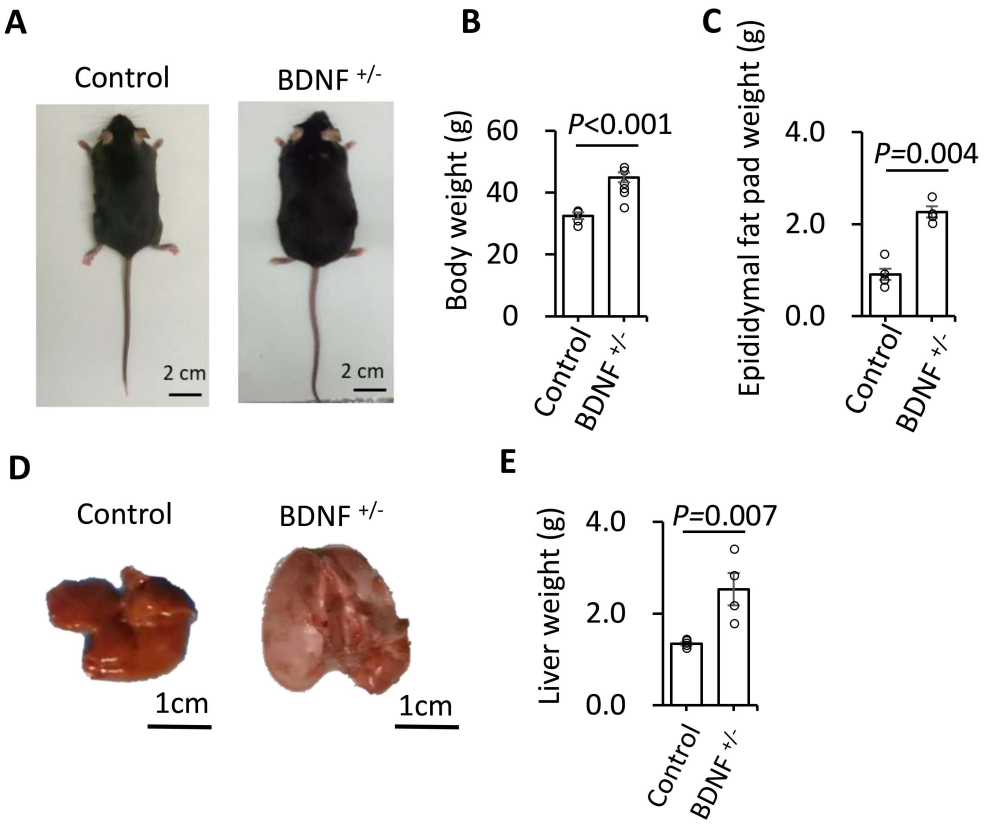
A
Control
BDNF +/-
2 cm
2 cm
B
Body weight (g)
60
40
20
0
P<0.001
Control
BDNF +/-
C
Epididymal fat pad weight (g)
4.0
2.0
0.0
P=0.004
Control
BDNF +/-
D
Control
BDNF +/-
1cm
1cm
E
Liver weight (g)
4.0
2.0
0.0
P=0.007
Control
BDNF +/-

Figure2

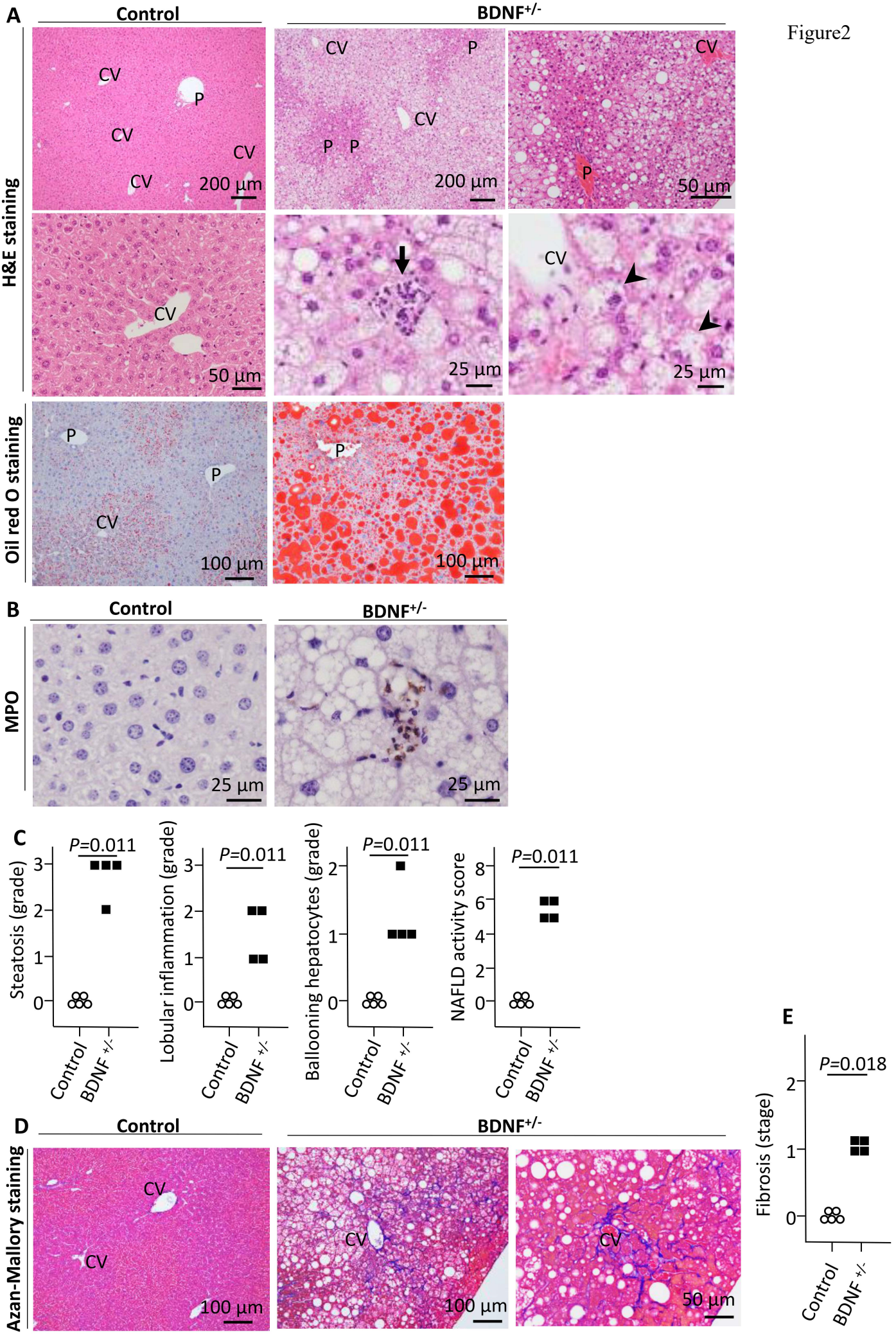
A
Control
BDNF+/-
H&E staining
CV
P
200 μm
50 μm
25 μm
Oil red O staining
100 μm
B
MPO
C
P=0.011
Steatosis (grade)
Lobular inflammation (grade)
Ballooning hepatocytes (grade)
NAFLD activity score
Control
BDNF +/-
D
Azan-Mallory staining
E
P=0.018
Fibrosis (stage)

Figure3

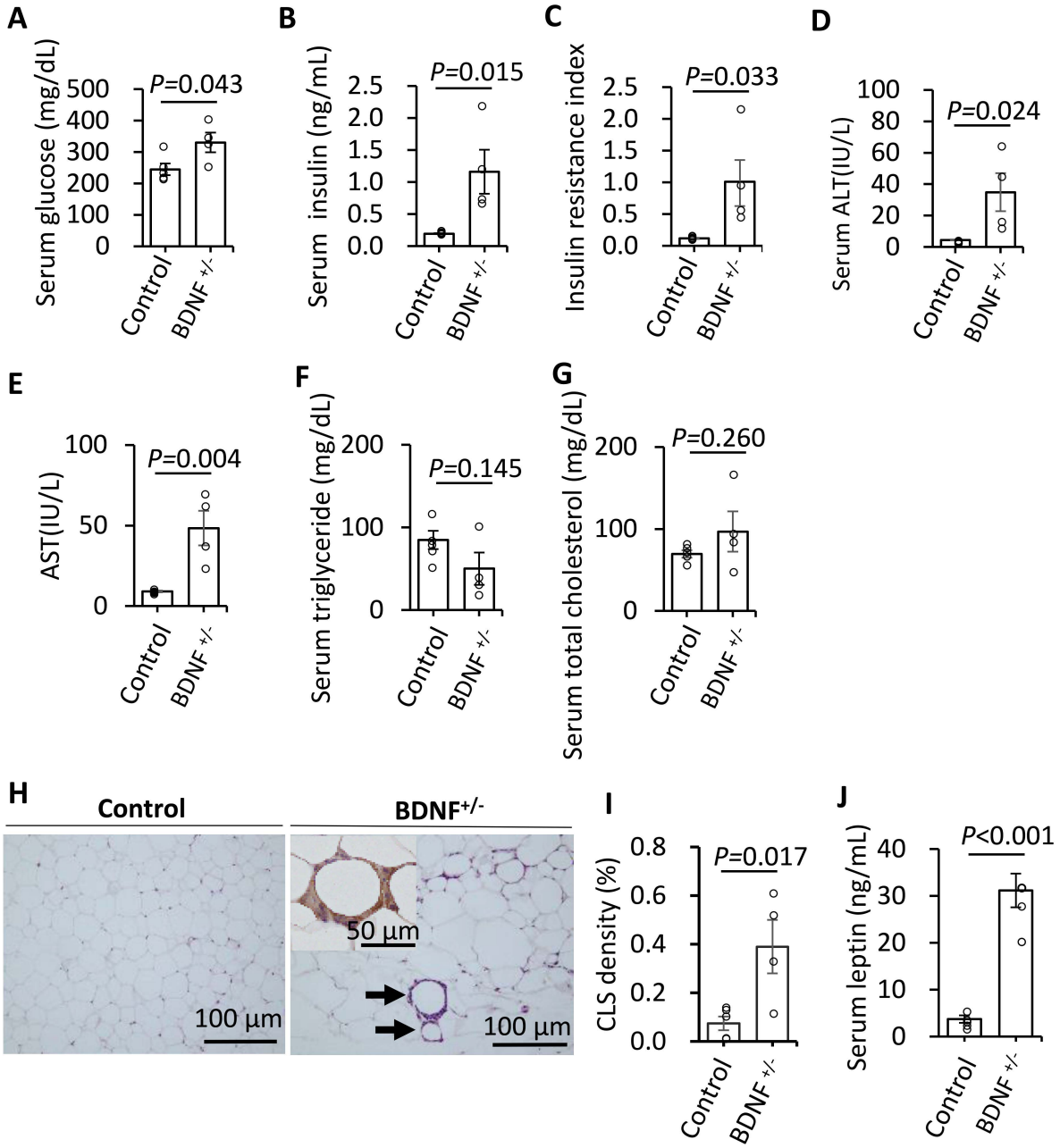
A
Serum glucose (mg/dL)
500
400
300
200
100
0
P=0.043
Control
BDNF +/-
B
Serum insulin (ng/mL)
2.5
2.0
1.5
1.0
0.5
0.0
P=0.015
Control
BDNF +/-
C
Insulin resistance index
2.5
2.0
1.5
1.0
0.5
0.0
P=0.033
Control
BDNF +/-
D
Serum ALT(IU/L)
100
80
60
40
20
0
P=0.024
Control
BDNF +/-
E
AST(IU/L)
100
50
0
P=0.004
Control
BDNF +/-
F
Serum triglyceride (mg/dL)
200
100
0
P=0.145
Control
BDNF +/-
G
Serum total cholesterol (mg/dL)
200
100
0
P=0.260
Control
BDNF +/-
H
Control
BDNF+/-
50 µm
100 µm
100 µm
I
CLS density (%)
0.8
0.6
0.4
0.2
0.0
P=0.017
Control
BDNF +/-
J
Serum leptin (ng/mL)
40
30
20
10
0
P<0.001
Control
BDNF +/-

Figure4

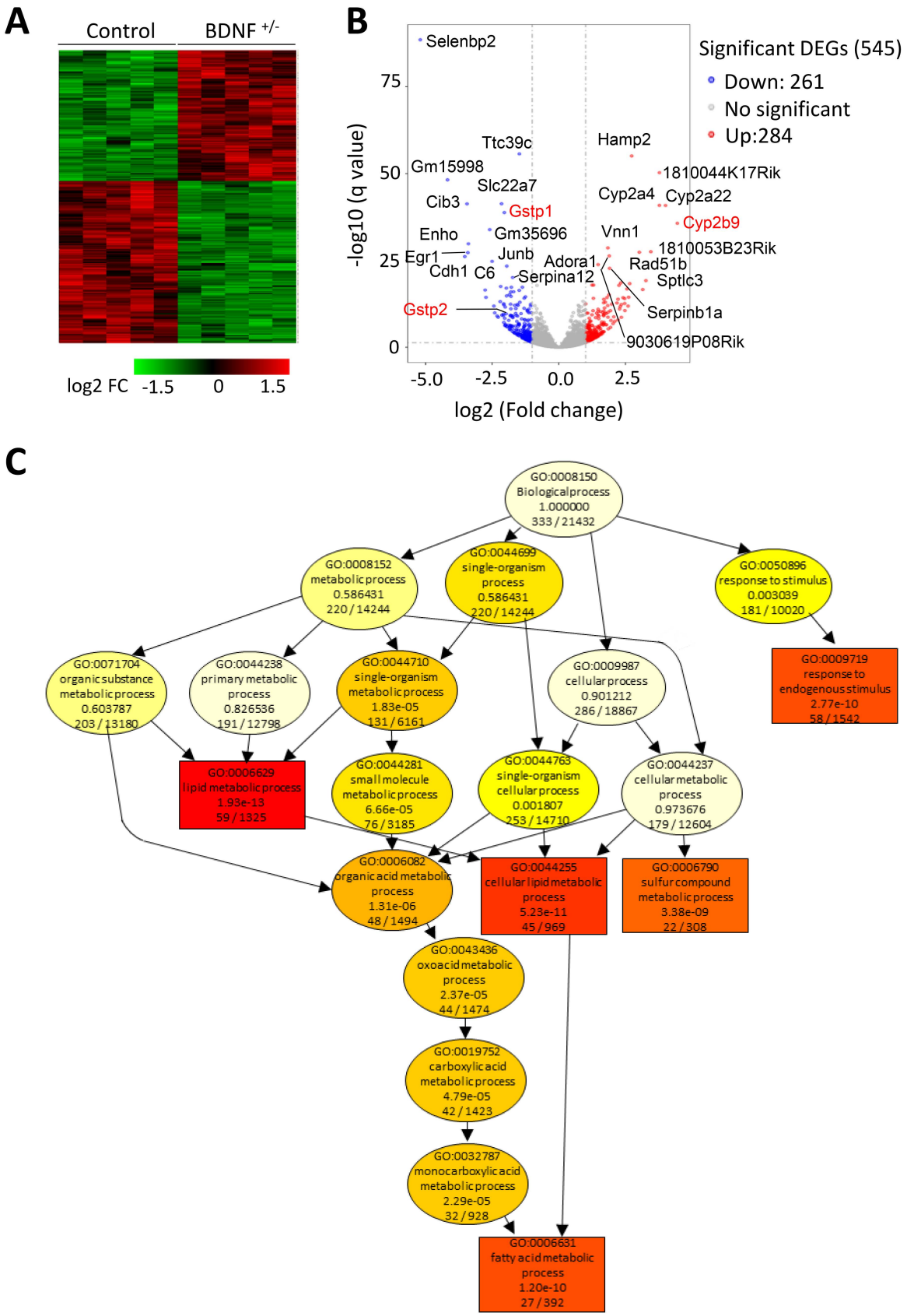
A
Control
BDNF +/-
log2 FC -1.5 0 1.5
B
Selenbp2
Ttc39c
Gm15998
Slc22a7
Cib3
Gstp1
Enho
Gm35696
Egr1
Junb
Cdh1
C6
Serpina12
Gstp2
Hamp2
1810044K17Rik
Cyp2a4
Cyp2a22
Cyp2b9
Vnn1
1810053B23Rik
Adora1
Rad51b
Sptlc3
Serpinb1a
9030619P08Rik
Significant DEGs (545)
Down: 261
No significant
Up:284
-log10 (q value)
log2 (Fold change)
C
GO:0008150 Biological process 1.000000 333 / 21432
GO:0008152 metabolic process 0.586431 220 / 14244
GO:0044699 single-organism process 0.586431 220 / 14244
GO:0050896 response to stimulus 0.003039 181 / 10020
GO:0071704 organic substance metabolic process 0.603787 203 / 13180
GO:0044238 primary metabolic process 0.826536 191 / 12798
GO:0044710 single-organism metabolic process 1.83e-05 131 / 6161
GO:0009987 cellular process 0.901212 286 / 18867
GO:0009719 response to endogenous stimulus 2.77e-10 58 / 1542
GO:0006629 lipid metabolic process 1.93e-13 59 / 1325
GO:0044281 small molecule metabolic process 6.66e-05 76 / 3185
GO:0044763 single-organism cellular process 0.001807 253 / 14710
GO:0044237 cellular metabolic process 0.973676 179 / 12604
GO:0006082 organic acid metabolic process 1.31e-06 48 / 1494
GO:0044255 cellular lipid metabolic process 5.23e-11 45 / 969
GO:0006790 sulfur compound metabolic process 3.38e-09 22 / 308
GO:0043436 oxoacid metabolic process 2.37e-05 44 / 1474
GO:0019752 carboxylic acid metabolic process 4.79e-05 42 / 1423
GO:0032787 monocarboxylic acid metabolic process 2.29e-05 32 / 928
GO:0006631 fatty acid metabolic process 1.20e-10 27 / 392

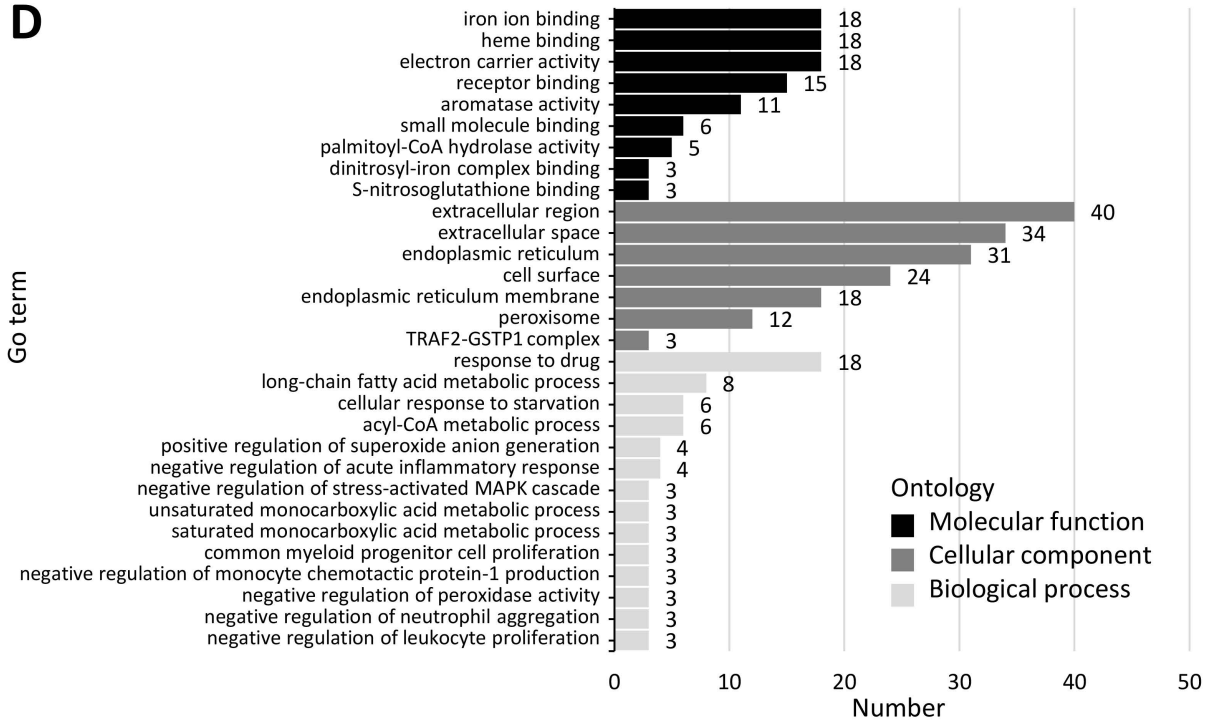
D
iron ion binding 18
heme binding 18
electron carrier activity 18
receptor binding 15
aromatase activity 11
small molecule binding 6
palmitoyl-CoA hydrolase activity 5
dinitrosyl-iron complex binding 3
S-nitrosoglutathione binding 3
extracellular region 40
extracellular space 34
endoplasmic reticulum 31
cell surface 24
endoplasmic reticulum membrane 18
peroxisome 12
TRAF2-GSTP1 complex 3
response to drug 18
long-chain fatty acid metabolic process 8
cellular response to starvation 6
acyl-CoA metabolic process 6
positive regulation of superoxide anion generation 4
negative regulation of acute inflammatory response 4
negative regulation of stress-activated MAPK cascade 3
unsaturated monocarboxylic acid metabolic process 3
saturated monocarboxylic acid metabolic process 3
common myeloid progenitor cell proliferation 3
negative regulation of monocyte chemotactic protein-1 production 3
negative regulation of peroxidase activity 3
negative regulation of neutrophil aggregation 3
negative regulation of leukocyte proliferation 3
Go term
Ontology
Molecular function
Cellular component
Biological process
0 10 20 30 40 50
Number

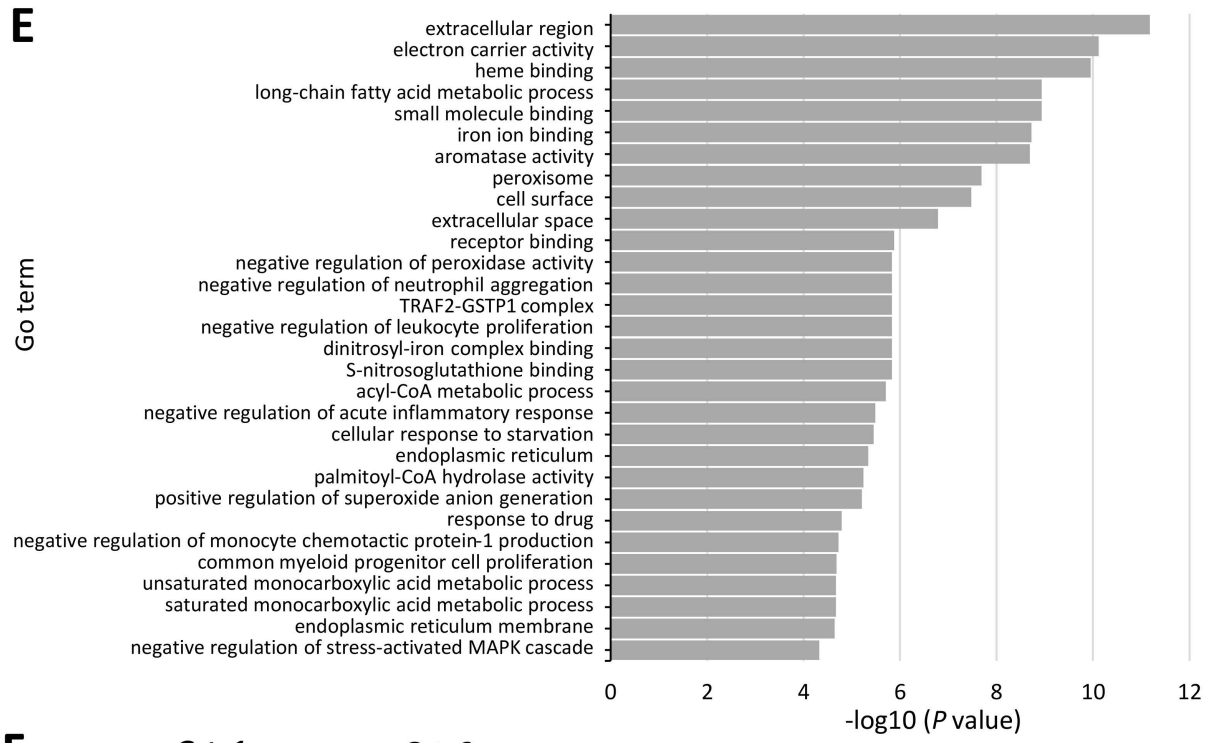
E
extracellular region
electron carrier activity
heme binding
long-chain fatty acid metabolic process
small molecule binding
iron ion binding
aromatase activity
peroxisome
cell surface
extracellular space
receptor binding
negative regulation of peroxidase activity
negative regulation of neutrophil aggregation
TRAF2-GSTP1 complex
negative regulation of leukocyte proliferation
dinitrosyl-iron complex binding
S-nitrosoglutathione binding
acyl-CoA metabolic process
negative regulation of acute inflammatory response
cellular response to starvation
endoplasmic reticulum
palmitoyl-CoA hydrolase activity
positive regulation of superoxide anion generation
response to drug
negative regulation of monocyte chemotactic protein-1 production
common myeloid progenitor cell proliferation
unsaturated monocarboxylic acid metabolic process
saturated monocarboxylic acid metabolic process
endoplasmic reticulum membrane
negative regulation of stress-activated MAPK cascade
Go term
0 2 4 6 8 10 12
-log10 (P value)

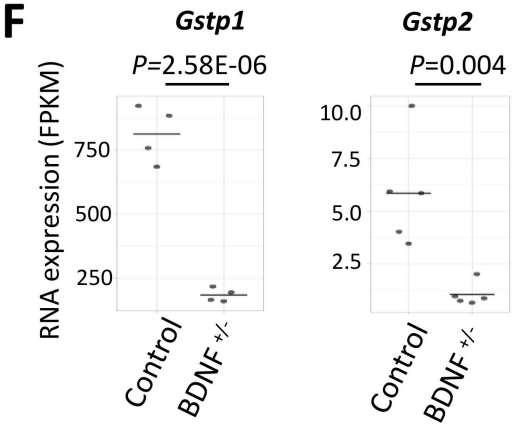
F
Gstp1
P=2.58E-06
Gstp2
P=0.004
RNA expression (FPKM)
750
500
250
10.0
7.5
5.0
2.5
Control
BDNF +/-
Control
BDNF +/-

Figure5

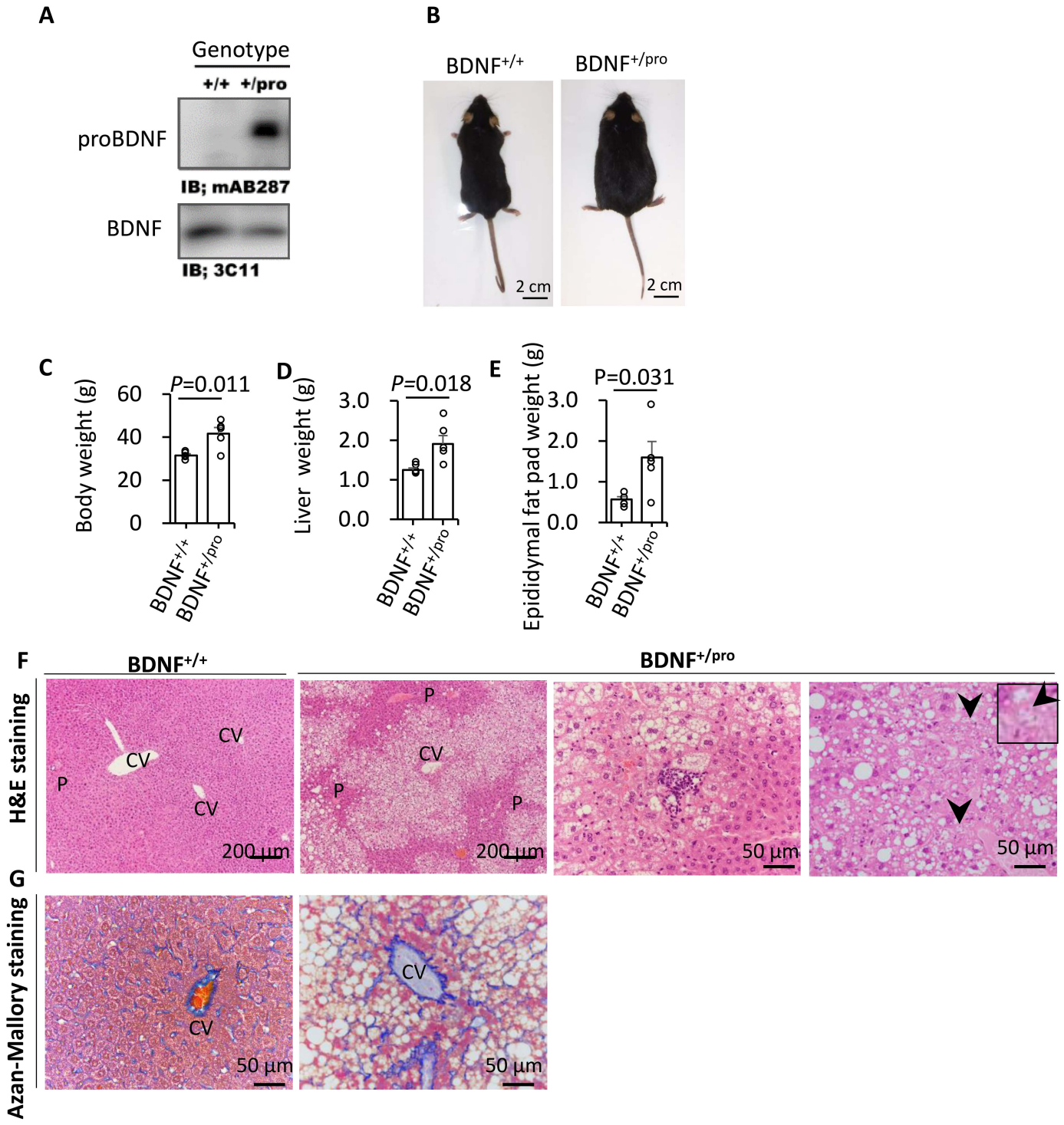
A
Genotype
+/+ +/pro
proBDNF
IB; mAB287
BDNF
IB; 3C11
B
BDNF+/+
BDNF+/pro
2 cm
2 cm
C
Body weight (g)
P=0.011
D
Liver weight (g)
P=0.018
E
Epididymal fat pad weight (g)
P=0.031
BDNF+/+
BDNF+/pro
F
BDNF+/+
BDNF+/pro
H&E staining
CV
P
200 µm
50 µm
G
Azan-Mallory staining
CV
50 µm

Figure6

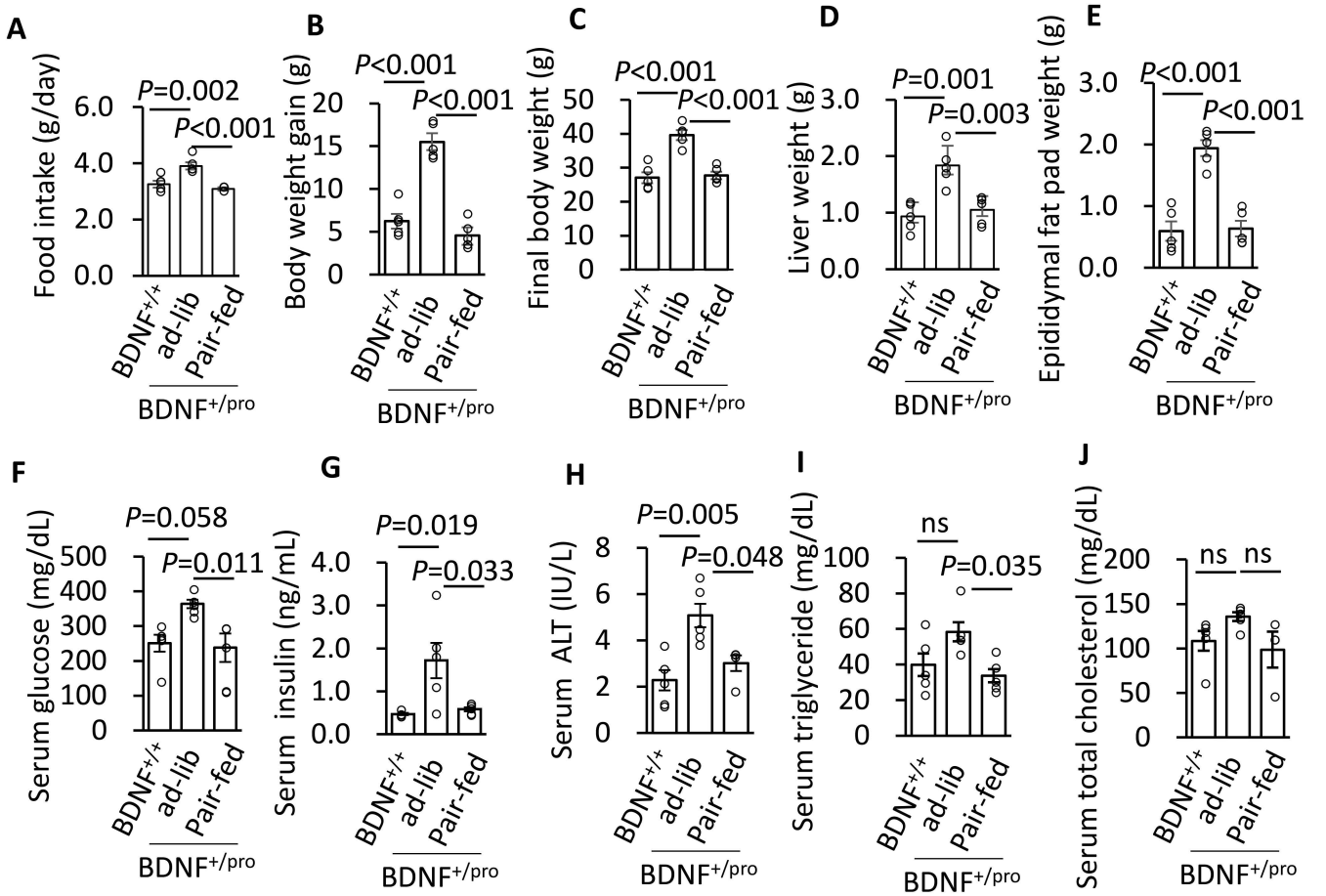
A
Food intake (g/day)
P=0.002
P<0.001
B
Body weight gain (g)
P<0.001
P<0.001
C
Final body weight (g)
P<0.001
P<0.001
D
Liver weight (g)
P=0.001
P=0.003
E
Epididymal fat pad weight (g)
P<0.001
P<0.001
BDNF+/+
ad-lib
Pair-fed
BDNF+/pro
F
Serum glucose (mg/dL)
P=0.058
P=0.011
G
Serum insulin (ng/mL)
P=0.019
P=0.033
H
Serum ALT (IU/L)
P=0.005
P=0.048
I
Serum triglyceride (mg/dL)
ns
P=0.035
J
Serum total cholesterol (mg/dL)
ns
ns

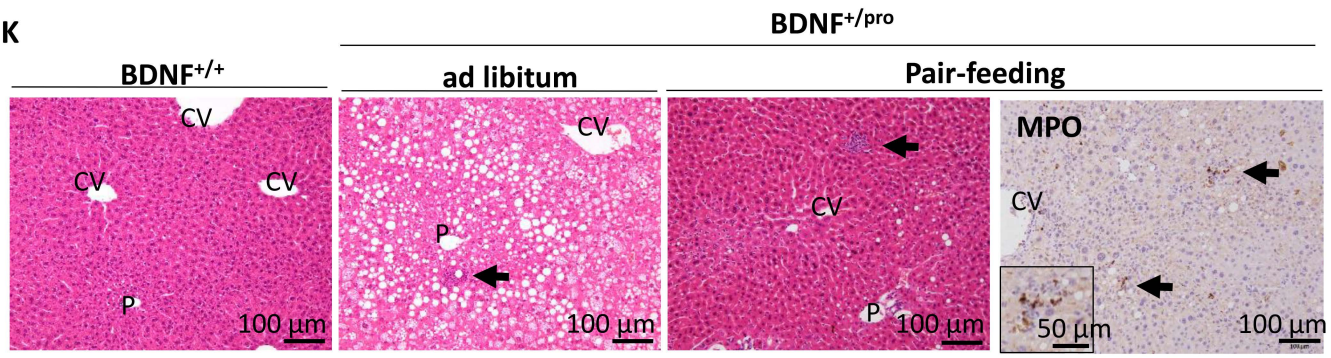
K
BDNF+/pro
BDNF+/+
ad libitum
Pair-feeding
CV
P
MPO
100 μm
50 μm

Supplementary Information

Supplementary Table Gene expression of cytochrome P450 family by RNA-seq analysis

	$BDNF^{+/-}$	Control	Relative ratio ($BDNF^{+/-}$/Control)	p value
Cyp1a2	140.3	279.1	0.50	0.001
Cyp2a12	223.2	172.2	1.30	0.001
Cyp2a4	9.0	0.4	24.96	0.001
Cyp2a21-ps	0.7	0.2	3.18	0.005
Cyp2a22	31.1	0.9	34.99	0.003
Cyp2b9	133.8	0.4	369.54	0.005
Cyp2b13	9.0	0.03	344.38	0.044
Cyp2c23	111.4	208.2	0.54	<0.001
Cyp2c38	59.5	15.6	3.81	0.002
Cyp2c39	6.8	0.6	10.93	0.034
Cyp2c39	6.8	0.6	10.93	0.034
Cyp2c40	7.0	1.9	3.78	0.043
Cyp2c53-ps	0.0	0.4	0.06	0.001
Cyp2c55	1.4	3.6	0.38	0.006
Cyp2c67	97.2	133.3	0.73	0.003

Cyp2c68	134.2	87.3	1.54	0.008
Cyp2c69	5.4	0.9	6.07	0.091
Cyp2c70	49.4	143.3	0.34	0.001
Cyp2d11	0.2	0.5	0.45	0.002
Cyp2d9	359.6	654.1	0.55	<0.001
Cyp2d41-ps	0.4	1.1	0.34	<0.001
Cyp2e1	4448.4	3191.0	1.39	0.003
Cyp2g1	0.3	0.5	0.51	0.031
Cyp2r1	4.3	6.7	0.65	0.029
Cyp2u1	5.1	9.2	0.56	0.002
Cyp3a25	403.0	528.8	0.76	0.039
Cyp4a10	1653.4	388.5	4.26	0.000
Cyp4a12a	80.2	140.6	0.57	0.036
Cyp4a12b	14.7	35.8	0.41	0.001
Cyp4a14	1550.8	243.0	6.38	0.002
Cyp4f14	31.6	64.1	0.49	0.004
Cyp4f39	0.1	0.2	0.55	0.010
Cyp7b1	31.3	131.5	0.24	<0.001
Cyp17a1	9.5	0.9	10.48	0.025
Cyp26a1	3.0	18.1	0.16	0.041

Cyp51	7.5	20.7	0.36	0.004

Data are mean of FPKM values. Number of animals used;5 (control) and 4 (BDNF+/-).

Cyp, cytochrome; ps, pseudogene.